Biophysical Chemistry 252 (2019) 106192

Contents lists available at ScienceDirect

Biophysical Chemistry

journal homepage: www.elsevier.com/locate/biophyschem

How do ribozymes accommodate additional water molecules upon hydrostatic compression deep into the kilobar pressure regime?

Narendra Kumar*, Dominik Marx

Lehrstuhl für Theoretische Chemie, Ruhr-Universität Bochum, 44780 Bochum, Germany

HIGHLIGHTS

- Hairpin ribozyme was simulated in explicit water by using replica-exchange molecular simulations at ambient and high hydrostatic pressure conditions.
- Hydrostatic compression has a negligible effect onto the H-bonding network of water molecules with the hairpin ribozyme.
- The interstitial water density significantly increases at multi-kilobar pressures, whereas the H-bonded water density remains largely unaffected.

GRAPHICAL ABSTRACT

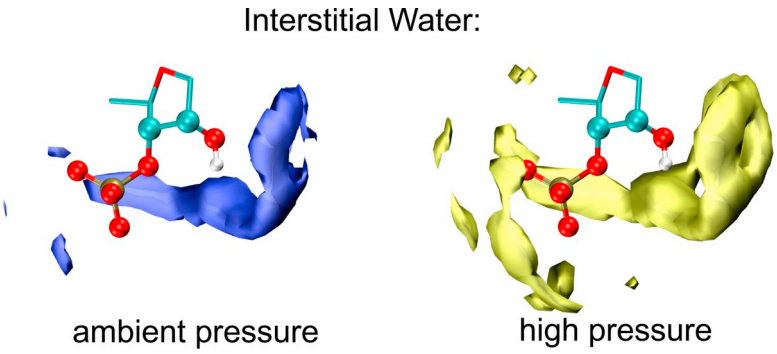

ARTICLE INFO

Keywords:
High-pressure conditions
Ribozymes
Hydrogen-bonding
Interstitial water
Replica-exchange molecular dynamics
RNA

ABSTRACT

Solvation by water plays an important role in the functional dynamics of biomacromolecules such as proteins or nucleic acids. This suggests that changes in solvation might drastically affect their functionality. Among other solvation stressors such as temperature, cosolvents or crowding agents, applying pressure in the multi-kilobar regime is known to modulate the hydration pattern of solutes, from simple to complex. In this study, we simulated a hairpin ribozyme, being catalytic RNA, using extensive replica-exchange molecular dynamics simulations at ambient and high hydrostatic pressure conditions. By dividing the coordinating water molecules present in the first solvation shell of the ribozyme into two subgroups, namely H-bonding and interstitial water, we discover that the H-bond network remains essentially unaffected even upon compression to 10 kbar compared to the 1 bar reference pressure. In stark contrast, the contribution of interstitial water significantly increases upon compression to 10 kbar, which discloses a differential effect of pressure perturbation on the solvation state of this ribozyme. In simple words: the increased water density due to compressing the aqueous ribozyme solution is locally accommodated by mainly pushing water molecules into the interstitial space offered by the existing H-bonding network of this RNA species. Given the molecularly generic nature of this finding, we expect it to hold true also for other biomacromolecules in aqueous solutions at high hydrostatic pressures, such as DNA or proteins.

* Corresponding author.
E-mail address: narendra.kumar@theochem.rub.de (N. Kumar).

https://doi.org/10.1016/j.bpc.2019.106192
Received 16 April 2019; Received in revised form 23 May 2019; Accepted 23 May 2019
Available online 25 May 2019

1. Introduction

Water is the universal solvent which supports all known forms of life. Its structural, dynamical and H-bonding properties are central to many processes from physics to chemistry to biology. In particular, it is now well established that water plays an integral role not only in the conformational dynamics, but also in folding and function of biomacromolecules such as proteins and nucleic acids [1–11]. The change in solvation of biomolecules affects their effective interactions with water thus their folding dynamics [12–16]. Since more recently, the solvation of biomolecules has been shown to change under high hydrostatic pressure (HHP) conditions [14,17,11,18], meaning upon entering the multi-kilobar hydrostatic compression regime. Among the driving ideas behind this line of research is that understanding biomolecules at such high pressures can elucidate the solvation not only of the low free energy states, but also provides insights into their excited conformational states, which are not much populated at in equilibrium at ambient conditions, yet highly relevant to dynamics and thus function [19–24].

More generally speaking, high-pressure research in biological systems [25,19,26–28,20–22,29,30,31,32,24] is tremendously important since pressure can serve as a control parameter to probe the thermodynamics and kinetics of biomolecular processes, for instance in the realm of folding and unfolding [33,23]. Pressure can be used to modulate biological activity [34], to induce or inhibit the formation of aggregates [35–37,31,32], and to modify the solvation [14,17,11,18]. Although high-pressure effects have been investigated thoroughly for proteins as extensively reviewed over the years [19,26,38,27,21,20,22,24] (see original literature therein), similar studies on nucleic acids such as RNAs are more scarce [39–50]. Therefore, in what follows, we focus on the pressure-induced molecular solvation changes of hairpin ribozyme, an RNA catalyst, based on our previous insights gained into its purely conformational pressure response [49,50].

Ribozymes are of immense interest in biology due to their putative role in early life at extreme conditions [51,52]. In general, ribozymes are non-coding RNAs which act as catalysts in biological reactions just as protein-based enzymes. Hairpin ribozyme catalyzes the site-specific self-cleavage of phosphodiester bonds which unlike other ribozymes does not require the presence of divalent metals ions in its active site [53–56]. This ribozyme consists of two domains dubbed domain A and domain B [55,57]. The reaction proceeds via formation of a complex where both domains come in close contact and form a so-called docked structure [58–61]. This docked structure [57] as depicted in Fig. 1 served us as the starting point for our simulation study.

In particular, studies have shown that highly structured water molecules are present at the active site of hairpin ribozyme which form a H-bonding network and are important for structural dynamics as well as catalytic functionality [62,63]. Studies have revealed that some of these water molecules might even be judiciously placed to shuttle protons in its self-cleavage reaction and, therefore, play an active role in this ribozymatic reaction at ambient conditions [57,8,64,65]. Moreover, the solvation of ribozymes and their catalytic functionality has been studied using pressure as a control parameter [44]. The changes in the conformation and solvation of the ribozyme is associated with a change in the volume which can be probed by applying high pressures [39]. Indeed, high-pressure studies have revealed a loss of water in the transition state [39,42]. Very recently, we have found that the self-cleavage step of the hairpin ribozyme is accelerated [49], whereas folding dynamics and docking of the loops, steps prior to self-cleavage as such, is decelerated under high-pressure conditions. Based on all this evidence, using pressure-induced perturbations of the solvation state of hairpin ribozyme might provide valuable insights into the role of water molecules in the folding dynamics and functionality of hairpin ribozyme or RNAs in general.

In this work, we investigate the solvation of the hairpin ribozyme especially in the context of how water molecules accommodate

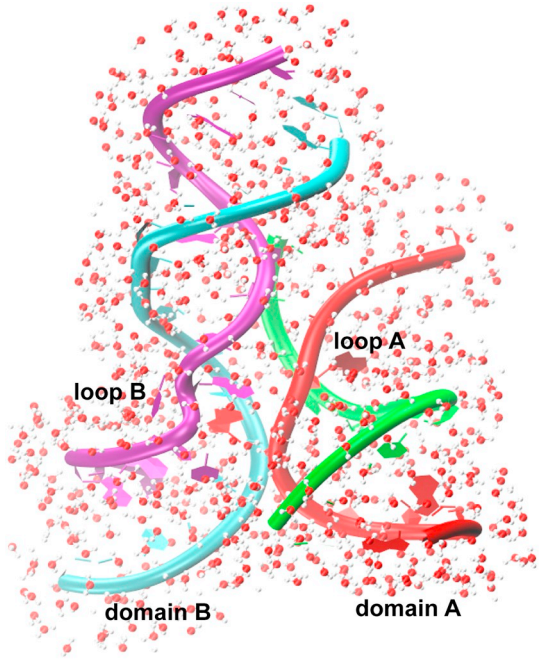

Fig. 1. Hairpin ribozyme structure based on PDB structure 2OUE [57] along with those water molecules that are within a distance of 3.5 Å from any atom of the ribozyme, thus roughly representing the first solvation shell of the ribozyme, from a representative molecular dynamics snapshot at 1 bar and 300 K.

themselves upon hydrostatic compression of the solution, and how the H-bonding network changes under high-pressure conditions. This is achieved based on extensive replica-exchange simulations using explicit water and physiological salt concentration at ambient as well as high-pressure conditions. The interactions are described in terms of an all-atom force field [66–68] (see Section 2.2 for details) that has been optimized and validated for RNA simulations [69–74], though some deficiencies still remain (for which we refer the interested reader to the original publications [75–77]).

2. Computational details and methods

2.1. Simulated system

Drawing on our earlier work [49,50], hairpin ribozyme was simulated in explicit water at finite salt concentrations and 300 K, both at ambient and high-pressure conditions. The initial structure of hairpin ribozyme was taken from the protein data bank (PDB), being structure 2OUE [57]. The missing hydrogen atoms were added and the methyl group at the 2′– oxygen of the A-1 nucleobase was replaced with a hydrogen atom, which provides the structure of hairpin ribozyme having all nucleobases in their respective canonical states. The ribozyme was solvated by explicitly adding water molecules and Na^+ and Cl^- ions as to neutralize the negatively charged ribozyme and to establish a salt concentration of 0.14 M at 1 kbar. The resulting system consisted of 44,346 atoms in total, including 1964 atoms of the ribozyme, 14,083 water molecules, 95 Na^+, and 38 Cl^- ions. The system was simulated at ambient and high-pressures of 1 bar and 10 kbar, respectively, using extensive temperature replica-exchange molecular dynamics simulations as to sufficiently sample the configurational space (see next subsections for more details).

In a previous simulation study [50] of the same ribozyme but devoted to different questions, we already carefully validated both, the stability of our system setup and the convergence of our statistical sampling of the relevant local conformational space using three different states (including the one that is used here) at both pressure

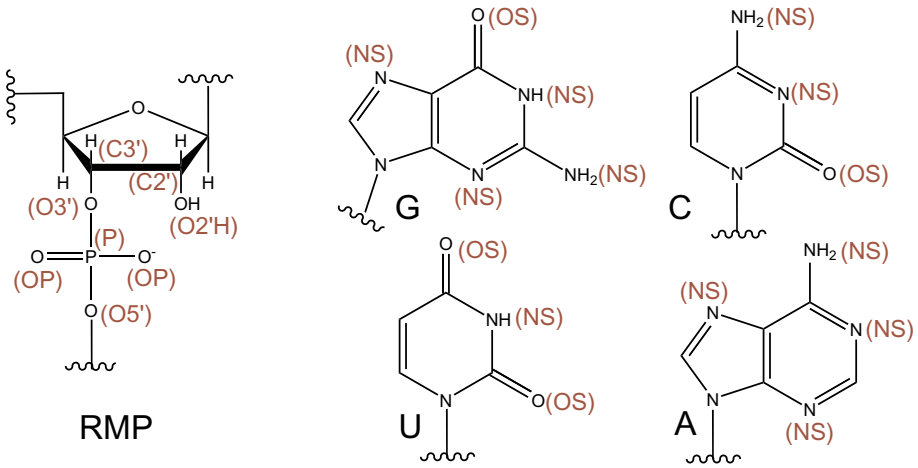

Fig. 2. The groups OP, O2′ H, NS, and OS shown here represent the oxygen atoms of non-bridging phosphate groups, 2′– hydroxyl groups, H-bonding nitrogen-based groups (i.e. $-NH_2$, $-NH-$, $=N-$), and the $=O$ groups of nucleobases of the hairpin ribozyme, respectively. RMP represents the ribose monophosphate unit whereas G, C, U, and A correspond to guanine, cytosine, uracil, and adenine, respectively.

Table 1
Number of H-bonded and interstitial water molecules OW (as well as their sum, "all") at 1 bar and 10 kbar at 300 K. Here, OP, O2′ H, NS, and OS represent the oxygen atoms of non-bridging phosphate groups, 2′ – hydroxyl groups, H-bonding nitrogen-based groups (i.e. $-NH_2$, $-NH-$, $=N-$), and the $=O$ groups of nucleobases (see Fig. 2), respectively, of the ribozyme. For reference purposes, these numbers are also computed taking into account exclusively the bulk water molecules in the ribozyme simulations (see text for definition) contributing the OW–OW data. The corresponding numbers from ab initio molecular dynamics simulations of neat bulk water (obtained from analyzing existing ab initio trajectories [17] using the present criteria) are labelled as OW^{ai}–OW^{ai}. The numbers in parentheses have been computed using only the second half of the available trajectories.

		1 bar	10 kbar	% Change
OP–OW	H-bonded	2.60 (2.60)	2.83 (2.80)	8.8
	Interstitial	0.83 (0.82)	1.21 (1.20)	45.8
	All	3.43 (3.42)	4.04 (4.00)	17.8
O2'H–OW	H-bonded	1.25 (1.26)	1.41 (1.45)	12.8
	Interstitial	1.11 (1.12)	1.76 (1.80)	58.6
	All	2.36 (2.38)	3.17 (3.25)	34.3
NS–OW	H-bonded	0.49 (0.50)	0.57 (0.58)	16.3
	Interstitial	0.38 (0.38)	0.65 (0.66)	71.1
	All	0.87 (0.88)	1.22 (1.24)	40.2
OS–OW	H-bonded	0.95 (0.94)	1.02 (1.02)	7.4
	Interstitial	0.92 (0.92)	1.39 (1.43)	51.1
	All	1.87 (1.86)	2.41 (2.45)	28.9
OW–OW	H-bonded	3.50 (3.51)	3.52 (3.52)	0.6
	Interstitial	1.50 (1.49)	3.60 (3.60)	140.0
	All	5.00 (5.00)	7.12 (7.12)	42.4
OW^{ai}–OW^{ai}	H-bonded	3.57 (3.57)	3.64 (3.64)	1.0
	Interstitial	1.54 (1.54)	3.77 (3.77)	144.8
	All	5.11 (5.11)	7.41 (7.41)	45.0

conditions, see Figs. 1 and 2 in the Electronic Supplementary Information of Ref. 50. In particular, taking only the second half of the available replica-exchange molecular dynamics trajectories provides the same Gibbs free energy landscapes as using twice that length, thus confirming local conformational convergence. Moreover, when computing the average number of H-bonded and interstitial water molecules around various groups (see below for context), we applied the same approach of using only the second half of the trajectories. The data reported in parentheses in Table 1 validate the convergence of our statistics also for these configurational observables which provide the basis for the present study.

2.2. Force field

We used the all-atom ff99bsc0χ_{OL3} force field [66–68] for the ribozyme. It has been extensively assessed in a number of studies to gain insights into structural and dynamical properties of RNAs or ribozymes [69–74] and found to allow for stable simulations at longer time scales [78,79,69–74]. Still, some remaining deficiencies have been reported recently [80,75–77] which remain yet to be analyzed thoroughly. Even in view of some remaining problems with state-of-the-art nucleic acid force fields, we are confident that the presently used one should be reliable for the purpose of present study where we do not analyze large-scale conformational fluctuations and dynamics of RNA, but rather local intermolecular contacts with water molecules. This is supported by recent studies where substantial agreement has been found with experimental findings [72,73,49,74] based on this approach. We used the TIP4P/2005 model to represent the water molecules in view of its good performance at the level of both, generating the phase diagram of ice [81] and describing the solvation of small biomolecules up to 10 kbar [82]. Finally, we took those force field parameters of Na^+ and Cl^- ions which have been specifically optimized for biomolecular simulations [83].

2.3. Preparation of the system and equilibration details

All simulations were performed using the Gromacs (version 5.0.2) simulation package [84,85] at *NpT* conditions within an orthorhombic box such that all atoms of the ribozyme molecule were at least 15 Å away from the edges of the periodic simulation supercell (which got filled with water). The leap-frog algorithm was used with an integration time step of 2 fs. The constant temperature and pressure conditions were maintained using the Nosé–Hoover thermostat [86,87] and the Parrinello–Rahman barrostat [88] with time constants of 1.5 and 1.0 ps, respectively, as implemented in Gromacs. The electrostatic interactions were treated using the smooth particle mesh Ewald method [89] with a real space cut-off of 12 Å; the distance to cut off the van der Waals interactions was also set to 12 Å. All covalent bonds involving hydrogen atoms were constrained using the LINCS algorithm [90].

A multi-step process was adopted to equilibrate the system as follows. First, the ribozyme was energy-minimized in vacuum using simple steepest descent for 2000 steps. Second, after solvating and adding ions as described above, the system was again energy-minimized for another 10,000 steps. Third, a 2 ns simulated annealing simulation was performed in the *NVT* ensemble where the system was first heated from 50 to 404 K at a rate of 0.5 K/ps. At 404 K, the system was equilibrated for another 500 ps and then was annealed down to 300 K at the same rate. At that target temperature, the system was equilibrated again for another 600 ps. At this stage, the system was further energy minimized for 10,000 steps followed by another 500 ps of *NVT* simulation at 300 K. This equilibrated system was finally used for the production run in the *NpT* ensemble at 1 bar. The high-pressure simulation setup was generated by increasing the pressure of that 1 bar system in

25 intermediate steps up to 10 kbar while equilibrating each of them for 500 ps.

2.4. Temperature replica-exchange

We used temperature replica-exchange molecular dynamics (T-REMD) simulations [91–93,41,94,95,76,48] to increase sampling of the configurational space. The T-REMD simulations were performed both at 1 bar and 10 kbar pressure. Each of the simulations consisted of 64 replicas covering the temperature range from 300 to 404 K. The optimized temperatures of these replicas were generated using a protocol [96] available at http://folding.bmc.uu.se/remd/. The generated temperatures of all 64 replicas are reported in Ref. [50].

The exchange of coordinates of adjacent replicas was attempted every 2 ps and the exchange probability was determined from [97].

$$P_{ex}(i \leftrightarrow j) = min(1, \exp((\beta_i - \beta_j)(U_i - U_j) + (\beta_i p_i - \beta_j p_j)(V_i - V_j)))$$

where $\beta_i = 1/k_B T_i$, T_i, U_i, p_i, and V_i is the temperature, potential energy, pressure, and volume of the system in replica i. The exchange probabilities for both systems were in the range of 20–30%. After the equilibration as described above, both systems were simulated each for 200 ns, thus providing us with a total of about 25 μs of sampling time.

2.5. Hydrogen bond definition

We adopted a standard geometric criterion to define H-bonding [98–101]. According to this well-established procedure, a H-bond exists if the distance between the donor and acceptor sites is less than or equal to 3.5 Å and the hydrogen–donor–acceptor angle is less than or equal to 30°. In the present study, we have calculated the H-bonds between different groups of the ribozyme and the water molecules as explained in the next section.

3. Results and discussion

3.1. H-bonded and interstitial water molecules

A bird's-eye view of the solvated hairpin ribozyme such as the representative snapshot provided by Fig. 1 at 1 bar unveils that water molecules are present at all sites, including loops and contact sites of the domains. Certainly, any pressure-induced change of the solvation state might impact on the folding or loop-loop dynamics of the ribozyme, and possibly even on its catalytic self-cleavage function. Therefore, in an effort to dissect the solvation structure, we divided the water molecules present within a 3.5 Å distance from H-bonding sites of the ribozyme (see below for definition and Fig. 2) into two classes, namely those water molecules which form H-bonds with such groups and non-H-bonded water molecules. The latter are located within the usual H-bonding distance (i.e. 3.5 Å) but do not form a H-bond with H-bonding groups of the ribozyme since the hydrogen–donor–acceptor angle is far from linearity as required for H-bonding. Following the literature, these specific solvent molecules are called “interstitial water molecules” [102] and have been shown to play a prominent role in the structure of bulk water and aqueous solutions at multi-kilobar pressures [17]. It is important to note that both, H-bonding and interstitial water molecules belong to the first solvation shell of the respective site, i.e. they are first-shell coordinating water molecules according to the usual nomenclature.

In hydrostatically compressed bulk water [17], the gross picture is that the three-dimensional locally tetrahedral H-bond network is preserved even at the highest possible compression of liquid water at 300 K, being roughly 10 kbar. The required total density increase of such maximally compressed water, as locally seen by the increased first-shell coordination number of the individual water molecules, is achieved by squeezing water molecules into the tetrahedral voids that are offered by the open tetrahedral H-bond network topology. Analyzing our available ab initio *NVE* molecular dynamics trajectories [17] based on the aforementioned criteria support that the number of H-bonded water molecules is close to pressure–independent upon compression from 1 bar to 10 kbar, see OW^{ai}–OW^{ai} data in Table 1. In stark contrast, the contribution of interstitial water molecules is found to increase very significantly according to the data compiled in Table 1. That phenomenon, therefore, is the reason behind both, the pronounced increase of the first-shell coordination number and the striking pressure-induced shape change in the region of the first and second maximum of the oxygen-oxygen radial distribution function of strongly compressed liquid bulk water (see Fig. 1b of Ref. 17). In neat bulk water, these interstitial water molecules have been shown to be mainly so-called “topological second to fourth H-bonded neighbors” [17].

The number density distribution functions of the oxygen atoms of water molecules (OW) with respect to four different H-bonding partner groups (OP, O2′ H, NS, OS) of the ribozyme at 300 K are analyzed at 10 kbar compared to 1 bar in Fig. 3. Here, OP, O2′ H, NS, and OS represent the oxygen atoms of non-bridging phosphate groups, 2′ – hydroxyl groups, H-bonding nitrogen-based groups (i.e. $-NH_2$, $-NH-$, $=N-$), and the $=O$ groups of nucleobases, respectively, of the ribozyme as illustrated schematically in Fig. 2. For each of the four H-bonding partners, the number density distributions have been computed for H-bonded and interstitial water molecules (both combined yield all coordinating water molecules in the first solvation shell of the respective group) at ambient and high-pressure conditions at 300 K; the corresponding number of H-bonded and interstitial water molecules around the different groups as well as the coordination number (“all”) is compiled in Table 1.

Before proceeding to analyze the pressure response of interstitial versus H-bonded water molecules close to hairpin ribozyme, we validate our approach relying on force field water (TIP4P/2005 model [81]) with respect to ab initio water (RPBE–D3 density functional [17]) in the limit of the neat bulk water. In the present force field simulations, the bulk water molecules are those that are located beyond the second solvation shell of the ribozyme. We conclude, based on comparing the bulk water data from the ribozyme simulations (OW–OW) to those based on the ab initio molecular dynamics [17] simulations (OW^{ai}–OW^{ai}) in Table 1, that the pressure response of the essentially homogeneous bulk water phase around the ribozyme is close to perfectly reproduced by the force field simulations.

At ambient pressure, the absolute interstitial water density around the non-bridging phosphate groups, i.e. the one corresponding to OP–OW pairs, is pretty small up to the respective H-bonding peak at about 2.65 Å compared to the pronounced water density stemming from H-bonded solvent molecules, see Fig. 3. In total, about 2.60 H-bonded but only $\approx$ 0.83 interstitial water molecules are found to solvate the OP groups according to the data in Table 1. The situation is quite different for the other three groups of potentially H-bonding sites of the ribozyme. Here, the relative contribution of interstitial water molecules is substantially higher than around the non-bridging phosphates (albeit the total number of both, H-bonded and interstitial water molecules, i.e. the coordination number, is considerably smaller in all three other cases). It is observed for all four groups considered that the relative contribution of interstitial water molecules is negligible for distances up to where the maximum of the first peak due to all coordinating water molecules is located, which is where most of the H-bonded water is accumulated. Thus, only beyond that distance is the contribution due to interstitial water setting in, which becomes increasingly more prominent as the contribution due to the H-bonded water molecules is quickly decaying toward zero for larger distances.

The interesting question now is how these different H-bonding groups of hairpin ribozyme respond to the compression of its aqueous solution to 10 kbar. In particular, how much does the number of H-bonded water molecules increase in view of the increased density and what is the role of interstitial water?

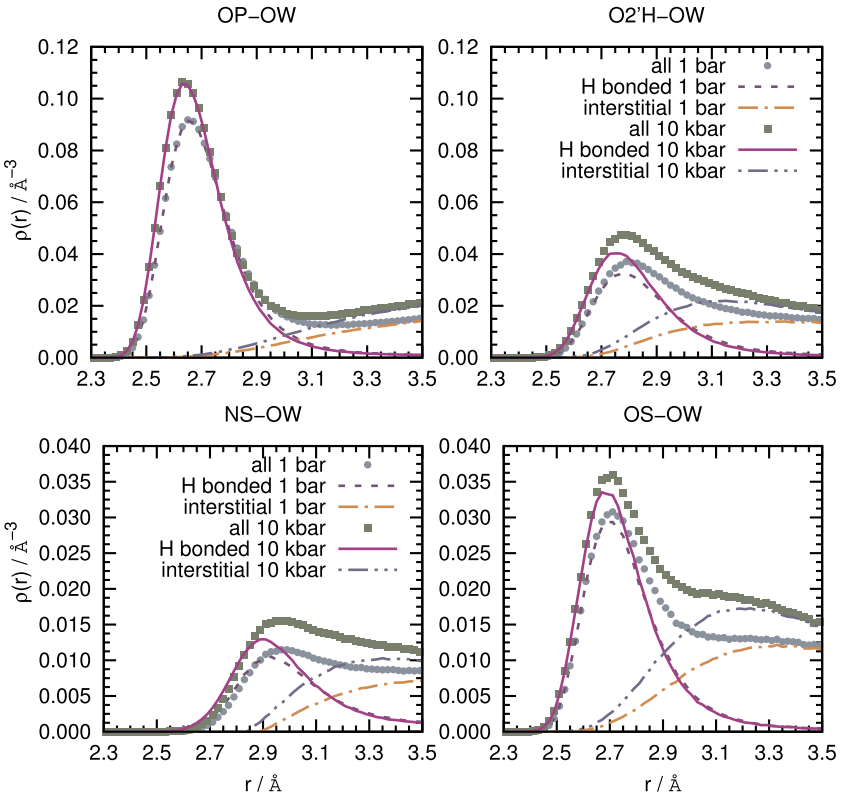

Fig. 3. Number density distributions, ρ(*r*), of water molecules (OW) with respect to four distinct H-bonding partner groups of the hairpin ribozyme (OP, O2′ H, NS, OS as defined in the text and shown in Fig. 2) split into H-bonded and interstitial water molecules compared to all coordinating first-shell water molecules at 1 bar and 10 kbar at 300 K; note the different density scales in the upper and lower panels.

3.2. Pressure effect on H-bonded and interstitial water densities

Upon inspection of Fig. 3, the first observation after compressing the solution from ambient to 10 kbar is that the total water density increases significantly in the first solvation shells of all four investigated functional groups of the ribozyme. This certainly does not come as a surprise but, secondly, it appears that the increase is significantly different in magnitude for H-bonded and interstitial water molecules. To investigate this further, we calculated the total number of H-bonding and interstitial water molecules (as collected in Table 1) by integrating the corresponding number density distributions over volume. This quantifies that the increase of the coordination numbers ("all") is in the range from about 20 to 40% depending on the specific group.

Much more important is the finding that the relative increase in the number of interstitial water molecules is much more pronounced than that for the H-bonding water molecules. This pressure-induced enhancement of interstitial water ranges from 45% in case of the phosphate groups up to 70% for the N–groups. In stark contrast, the H-bonding around all four groups is rather inert to compression into the kilobar regime, featuring an increase of H-bonded water molecules corresponding to roughly 10% only. This is a very interesting finding as it shows that, under high-pressure conditions, the increase in water density close to functional groups of the ribozyme, as seen by an increased coordination number of its H-bonding groups, mostly leads to an enhanced number of interstitial water molecules in their first solvation shells, whereas the H-bonding network of the ribozyme is only little affected.

How do these pressure-induced changes in the first solvation shell of hairpin ribozyme compare to those in the first solvation shell of a water molecule in bulk water? To quantify the effect of pressure on H-bonded and interstitial water densities in the bulk water phase that hosts the ribozyme, we present the corresponding number density distribution functions in Fig. 5 (leading to the OW–OW data in Table 1 upon integration) using the same criteria as applied to the ribozyme. Overall, we observe a similar effect in bulk water upon compression to 10 kbar, however, in comparison to the H-bonding groups of the ribozyme, the relative increase in interstitial and H–bonded water molecules is significantly higher and lower, respectively, in the bulk phase according to Table 1. Still, the major pressure-induced increase of the number of coordinating water molecules in the first-solvation shell of hairpin ribozyme overwhelmingly comes from enhancing the contribution of interstitial water compared to H-bonded water according to the data sets reported in Table 1.

A three-dimensional picture of the relative increase of the interstitial water with respect to H-bonded water is provided by the spatial distribution functions (SDFs) of oxygen atoms of the respective water molecules around the important H-bonding groups of the hairpin ribozyme at 10 kbar versus 1 bar (Fig. 4); the common reference frame for all SDFs is defined by the O2′–C2′–C3′–O3′–P–O5′ chain as shown in Fig. 2. The SDFs are shown for the same isovalue at 1 bar and 10 kbar pressure conditions, both at 300 K, and have been averaged taking into account all 57 respective sites offered by our computational model of the ribozyme by suitably translating and rotating them into the common reference frame (while excluding the terminal sites which are subject to large-amplitude fluctuations). Comparing the top-left to the top-central SDF discloses that not only the number of H-bonding molecules (as already known from Table 1), but also their positions relative to the ribozyme, as quantified by the shape of the isosurface in three-dimensional space, remains unaffected by the compression from ambient (blue isosurface) to 10 kbar (yellow isosurface) pressure. Direct superposition of these two isosurfaces, contributed in the top-right panel, provides essentially fully overlapping spatial populations of those water molecules that are H-bonded to the ribozyme. The picture is vastly different for interstitial water (see bottom panels). In this case, the isosurface at 10 kbar (bottom-central) encloses much larger regions in space than at 1 bar (bottom-left), which is nicely supported by the bottom-right superposition. This spatial analysis provides conclusive support of our finding that the H-bonding network is largely unaffected by compression, whereas the number of interstitial water molecules is significantly enhanced at 10 kbar.

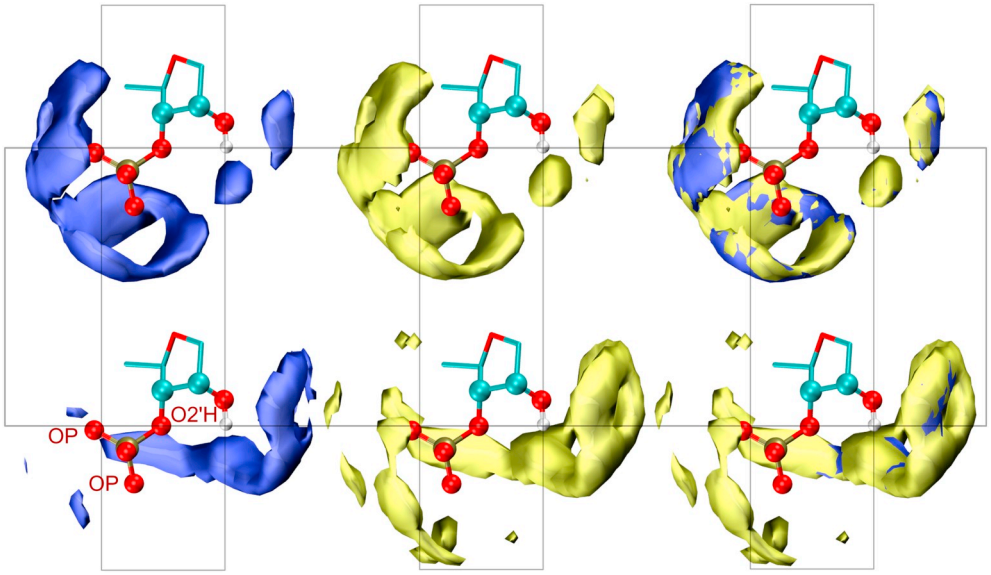

Fig. 4. Spatial distribution functions, SDFs, of oxygen atoms of H-bonded (top row) and interstitial (bottom row) water molecules around the important H-bonding groups of the hairpin ribozyme at 300 K. The blue and yellow colors represent 1 bar (left column) and 10 kbar (central column) pressure conditions, respectively, and transparent rectangles are included to guide the eye when comparing the SDFs in detail. The 1 bar and 10 kbar SDFs are superimposed in the right column for one-to-one comparison. (For interpretation of the references to colour in this figure legend, the reader is referred to the web version of this article.)

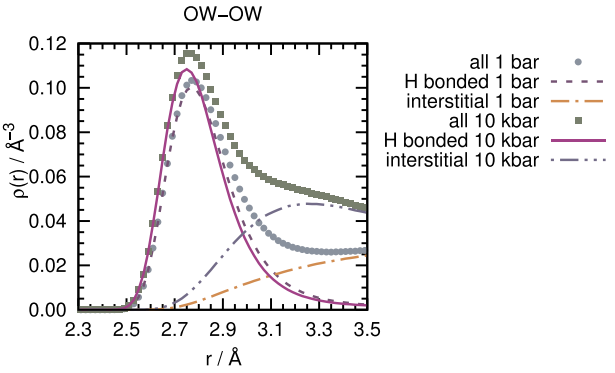

Fig. 5. Number density distributions, ρ(*r*), of water molecules (OW) in the bulk water phase around hairpin ribozyme split into H-bonded and interstitial water molecules compared to all coordinating first-shell water molecules at 1 bar and 10 kbar at 300 K.

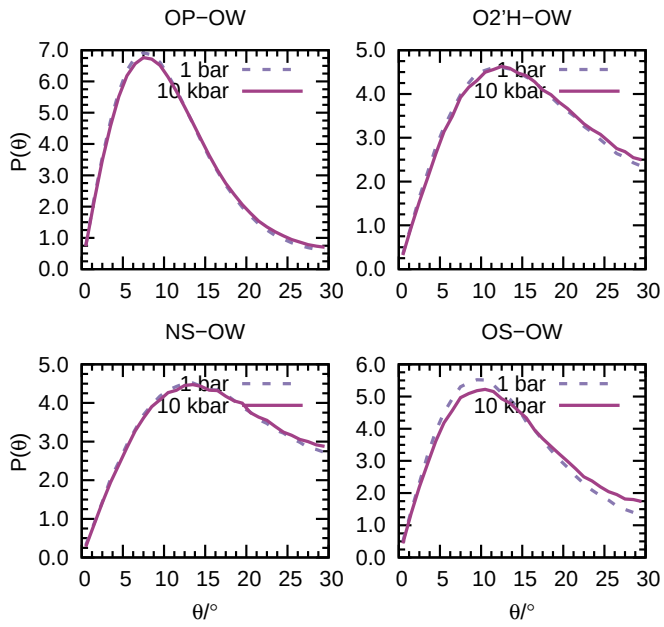

Fig. 6. Angle distribution, P(*θ*), of H-bonded water molecules with respect to four distinct H-bonding partner groups of the hairpin ribozyme (OP, O2′H, NS, OS as defined in the text and shown in Fig. 2) at 1 bar and 10 kbar at 300 K. Here, *θ* represent the hydrogen–donor–acceptor angle.

3.3. Pressure effect on H-bonding interaction strength

Roughly speaking, the strength of H-bonds correlates with their length and linearity, being the stronger the shorter and the more linear they are [103–105,99,106]. This qualitative correlation actually supports the use of very simple geometric criteria to define H-bonds at the level of these two structural parameters [98–101]. Therefore, in an effort qualitatively assess the impact of pressure on the strength of the H-bonding interactions of hairpin ribozyme in water, we analyzed the hydrogen–donor–acceptor angle (Fig. 6) as well as the donor–acceptor distance (Fig. 7) distribution functions of only the H-bonded water molecules around the ribozyme at 300 K. Inspecting the H-bond angle distribution functions from Fig. 6 for all four H-bonding groups shows that they barely change upon compressing the aqueous solution to 10 kbar. Most notably, the most probable value of the H-bond angle is virtually pressure insensitive for all H-bonding sites offered by the ribozyme. Next, the donor-acceptor distance distributions (note that these are not radial distribution functions) of these H-bonding sites also do not change much upon compression according to the data in Fig. 7. The corresponding most probable H-bond lengths are systematically shorter at 10 kbar compared to ambient pressure, but only by roughly −0.02 Å which is a marginal ~1 % effect.

The key conclusion from this final piece of our analysis is that not only the gross H-bonding structure around the hairpin ribozyme remains largely unaffected upon compression to 10 kbar, but also the H-bond interaction strengths as assessed by using two suitable structural proxies are rather pressure-independent in the multi-kilobar compression regime.

4. Conclusions and outlook

The pressure response of hairpin ribozyme in water at 300 K has been dissected at the level of its molecular solvation properties at 10 kbar versus ambient pressure, 1 bar; note that 10 kbar is close to the stability limit of neat liquid water at room temperature. This is achieved by using extensive replica-exchange molecular dynamics simulations of this RNA system in explicit water, generating a total of roughly 25 *μs* of sampling time allowing for comprehensive statistical analyses of configurations at the molecular level.

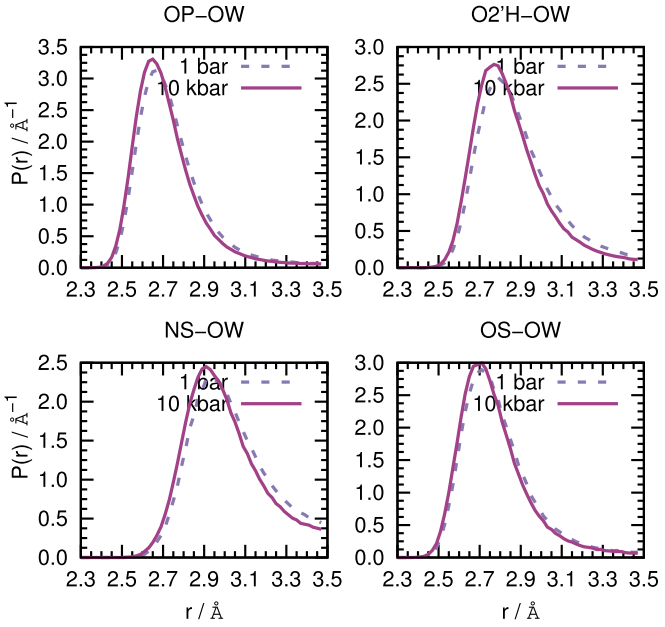

Fig. 7. Distance distribution, P(r), of H-bonded water molecules with respect to four distinct H-bonding partner groups of the hairpin ribozyme (OP, O2′H, NS, OS as defined in the text and shown in Fig. 2) at 1 bar and 10 kbar at 300 K. Here, r represents the donor–acceptor distance.

Stimulated by our recent insights into the pressure response of both, neat bulk water and aqueous solutions of simple molecules such as TMAO when hydrostatically compressed to 10 kbar, we divided the water molecules present in the first hydration shell into two subgroups, being the H-bonded and interstitial water molecules. Only the former do form a H-bond with potentially H-bonding sites of the ribozyme, such as phosphate or carbonyl oxygens acting as acceptors or nitrogen groups serving as potential H-bond donors. The interstitial water molecules are also first-shell neighbors of the respective interaction sites, but they are only populating void space that is left open by the H-bonded first neighbors of those sites, and are therefore not H-bonded to the respective sites. It is the sum of H-bonded and interstitial solvent molecules in the first solvation shell of a given solvation site that provides its coordination number.

Careful analysis of various structure-based observables unveils that the average H-bond pattern around each and every of the potentially H-bonding sites of the ribozyme is only little affected by pressures as extreme as 10 kbar. This includes the arrangement of these H-bonded water molecules in three-dimensional space and also the H-bonding interaction strength as qualitatively assessed by exploiting its correlation with H-bond lengths and angles. In stark contrast, the relative contribution of interstitial water is strongly enhanced around all H-bonding sites of the ribozyme at 10 kbar with direct reference to the scenario at 1 bar. Overall, the increased coordination number of H-bonding sites of hairpin ribozyme due to hydrostatic compression is not achieved by enhancing the number of H-bonds, but rather by squeezing non-H-bonded water molecules in between the H-bonded water molecules, thereby filling at high pressures that interstitial space which is unoccupied at ambient conditions.

Having disclosed a clearly differential effect of pressure perturbation on the solvation state of this particular ribozyme, an interesting next step would be to find out if there is pressure-dependent impact on forming the docked state, on undocking or even on the self-catalyzed cleavage reaction of this ribozyme. Beyond hairpin ribozyme, we expect that not only other RNA or DNA constructs, such as tetraloops or quadruplexes, but also hydration of proteins in general and enzymes in particular will respond to pressure-induced solvation stress using the same molecular mechanism to locally deal with enhanced water densities via interstitial water.

Acknowledgment

It gives us great pleasure to thank Roland Winter, Caroline Schuabb, Salome Pataraia, as well as Satyajit Patra for fruitful discussions on experimental aspects of the pressure response of hairpin ribozyme. We also would like to thank Sho Imoto for assistance with the ab initio reference trajectories of neat bulk water. Financial support from the Deutsche Forschungsgemeinschaft (DFG) Research Unit FOR 1979 “Exploring the Dynamical Landscape of Biomolecular Systems by Pressure Perturbation” (MA 1547/17) is gratefully acknowledged and the project is also part of the Cluster of Excellence RESOLV (EXC 2033, ID 390677874) funded as well by the DFG. The simulations have been carried out on HPC-RESOLV, HPC@ZEMOS, BOVILAB@RUB and RV-NRW platforms.

References

[1] I. Ohmine, H. Tanaka, Fluctuation, relaxations, and hydration in liquid water. Hydrogen-bond rearrangement dynamics, Chem. Rev. 93 (1993) 2545–2566.
[2] V.V. Mozhaev, K. Heremans, J. Frank, P. Masson, C. Balny, High pressure effects on protein structure and function, Proteins Struct. Funct. Genet. 24 (1996) 81–91.
[3] D. Beveridge, K.J. McConnell, Nucleic acids: theory and computer simulation, Y2K, Curr. Opin. Struct. Biol. 10 (2000) 182–196.
[4] P. Auffinger, E. Westhof, Hydrophobic groups stabilize the hydration shell of 2'-O-methylated RNA duplexes, Angew. Chem. Int. Ed. Eng. 40 (2001) 4648–4650.
[5] P. Auffinger, E. Westhof, RNA solvation: a molecular dynamics simulation perspective, Biopolymers 56 (2000) 266–274.
[6] K. Réblová, N. Spacková, J.E. Šponer, J. Koca, J. Šponer, Molecular dynamics simulations of RNA kissing-loop motifs reveal structural dynamics and formation of cation-binding pockets, Nucleic Acids Res. 31 (2003) 6942–6952.
[7] E.J. Sorin, Y.M. Rhee, V.S. Pande, Does water play a structural role in the folding of small nucleic acids? Biophys. J. 88 (2005) 2516–2524.
[8] H. Park, S. Lee, Role of solvent dynamics in stabilizing the transition state of RNA hydrolysis by hairpin ribozyme, J. Chem. Theory Comput. 2 (2006) 858–862.
[9] M.V. Krasovska, J. Sefcikova, K. Réblová, B. Schneider, N.G. Walter, J. Šponer, Cations and hydration in catalytic RNA: molecular dynamics of the hepatitis delta virus ribozyme, Biophys. J. 91 (2006) 626–638.
[10] P. Ball, Water as an active constituent in cell biology, Chem. Rev. 108 (2008) 74–108.
[11] L. Biedermannová, B. Schneider, Hydration of proteins and nucleic acids: advances in experiment and theory. A review, Biochim. Biophys. Acta 1860 (2016) 1821–1835.
[12] D. Paschek, S. Gnanakaran, A.E. Garcia, Simulations of the pressure and temperature unfolding of an α-helical peptide, Proc. Natl. Acad. Sci. U. S. A. 102 (2005) 6765–6770.
[13] T. Imai, Y. Sugita, Dynamic correlation between pressure-induced protein structural transition and water penetration, J. Phys. Chem. B 114 (2010) 2281–2286.
[14] J. Roche, J.A. Caro, D.R. Norberto, P. Barthe, C. Roumestand, J.L. Schlessman, A.E. Garcia, B. Garcia-Moreno, C.A. Royer, Cavities determine the pressure unfolding of proteins, Proc. Natl. Acad. Sci. U. S. A. 109 (2012) 6945–6950.
[15] Y. Mori, H. Okumura, Molecular dynamics of the structural changes of helical peptides induced by pressure, proteins Struct. Funct, Bioinforma 82 (2014) 2970–2981.
[16] D. Russo, A. Laloni, A. Filabozzi, M. Heyden, Pressure effects on collective density fluctuations in water and protein solutions, Proc. Natl. Acad. Sci. U. S. A. 114 (2017) 11410–11415.
[17] S. Imoto, H. Forbert, D. Marx, Water structure and solvation of osmolytes at high hydrostatic pressure: pure water and TMAO solutions at 10 kbar versus 1 bar, Phys. Chem. Chem. Phys. 17 (2015) 24224–24237.
[18] S. Imoto, P. Kibies, C. Rosin, R. Winter, S.M. Kast, D. Marx, Toward extreme biophysics: deciphering the infrared response of biomolecular solutions at high pressures, Angew. Chem. Int. Ed. 55 (2016) 9534–9538.
[19] K. Akasaka, Probing conformational fluctuation of proteins by pressure perturbation, Chem. Rev. 106 (2006) 1814–1835.
[20] K. Akasaka, R. Kitahara, Y.O. Kamatari, Exploring the folding energy landscape with pressure, Arch. Biochem. Biophys. 531 (2013) 110–115.
[21] F. Meersman, I. Daniel, D.H. Bartlett, R. Winter, R. Hazael, P.F. McMillan, High-pressure biochemistry and biophysics, Rev. Mineral. Geochem. 75 (2013) 607–648.
[22] J.L. Silva, A.C. Oliveira, T.C.R.G. Vieira, G.A.P. de Oliveira, M.C. Suarez, D. Foguel, High-pressure chemical biology and biotechnology, Chem. Rev. 114 (2014) 7239–7267.
[23] T.Q. Luong, S. Kapoor, R. Winter, Pressure - a gateway to fundamental insights into protein solvation, dynamics, and function, ChemPhysChem 16 (2015) 3555–3571.
[24] R. Winter, Interrogating the structural dynamics and energetics of biomolecular systems with pressure modulation, Annu. Rev. Biophys. 48 (2019) 441–463.

[25] M. Iwadate, T. Asakura, P.V. Dubovskii, H. Yamada, K. Akasaka, M.P. Williamson, Pressure-dependent changes in the structure of the melittin alpha-helix determined by NMR, J. Biomol. NMR 19 (2001) 115–124.
[26] D.H. Bartlett, Introduction to high-pressure bioscience and biotechnology, Ann. N. Y. Acad. Sci. 1189 (2010) 1–5.
[27] G. Demazeau, N. Rivalain, The development of high hydrostatic pressure processes as an alternative to other pathogen reduction methods, J. Appl. Microbiol. 110 (2011) 1359–1369.
[28] S. Kapoor, G. Triola, I.R. Vetter, M. Erlkamp, H. Waldmann, R. Winter, Revealing conformational substates of lipidated N-Ras protein by pressure modulation, Proc. Natl. Acad. Sci. U. S. A. 109 (2012) 460–465.
[29] S. Suladze, S. Cinar, B. Sperlich, R. Winter, Pressure modulation of the enzymatic activity of phospholipase A2, a putative membrane-associated pressure sensor, J. Am. Chem. Soc. 137 (2015) 12588–12596.
[30] E. Decaneto, S. Suladze, C. Rosin, M. Havenith, W. Lubitz, R. Winter, Pressure and temperature effects on the activity and structure of the catalytic domain of human MT1-MMP, Biophys. J. 109 (2015) 2371–2381.
[31] M.W. Jaworek, V. Schuabb, R. Winter, Pressure and cosolvent modulation of the catalytic activity of amyloid fibrils, Chem. Commun. 54 (2018) 5696–5699.
[32] K. Sakurai, A. Maeno, Y.H. Lee, K. Akasaka, Conformational properties relevant to the amyloidogenicity of beta2-microglobulin analyzed using pressure- and salt-dependent chemical shift data, J. Phys. Chem. B 123 (2019) 836–844.
[33] F. Meersman, P.F. McMillan, High hydrostatic pressure: a probing tool and a necessary parameter in biophysical chemistry, Chem. Commun. 50 (2014) 766–775.
[34] A.A. Makarov, R. Helmy, L. Joyce, M. Reibarkh, M. Maust, S. Ren, I. Mergelsberg, C.J. Welch, Use of hydrostatic pressure for modulation of protein chemical modification and enzymatic selectivity, Org. Biomol. Chem. 14 (2016) 4448–4455.
[35] R.J. St. John, J.F. Carpenter, T.W. Randolph, High pressure fosters protein refolding from aggregates at high concentrations, Proc. Natl. Acad. Sci. U. S. A. 96 (1999) 13029–13033.
[36] W. Dzwolak, R. Ravindra, J. Lendermann, R. Winter, Aggregation of bovine insulin probed by DSC/PPC calorimetry and FTIR spectroscopy, Biochemistry 42 (2003) 11347–11355.
[37] R. Jansen, S. Grudzielanek, W. Dzwolak, R. Winter, High pressure promotes circularly shaped insulin amyloid, J. Mol. Biol. 338 (2004) 203–206.
[38] G. Demazeau, N. Rivalain, High hydrostatic pressure and biology: a brief history, Appl. Microbiol. Biotechnol. 89 (2011) 1305–1314.
[39] S. Tobé, T. Heams, J. Vergne, G. Hervé, M.-C. Maurel, The catalytic mechanism of hairpin ribozyme studied by hydrostatic pressure, Nucleic Acids Res. 33 (2005) 2557–2564.
[40] G. Hervé, S. Tobé, T. Heams, J. Vergne, M.-C. Maurel, Hydrostatic and osmotic pressure study of the hairpin ribozyme, Biochim. Biophys. Acta, Proteins Proteomics 1764 (2006) 573–577.
[41] A.E. Garcia, D. Paschek, Simulation of the pressure and temperature folding/unfolding equilibrium of a small RNA hairpin, J. Am. Chem. Soc. 130 (2008) 815–817.
[42] M. Ztouti, H. Kaddour, F. Miralles, C. Simian, J. Vergne, G. Hervé, M.-C. Maurel, Adenine, a hairpin ribozyme cofactor-high-pressure and competition studies, FEBS J. 276 (2009) 2574–2588.
[43] D.N. Dubins, A. Lee, R.B. Macgregor, T.V. Chalikian, On the stability of double stranded nucleic acids, J. Am. Chem. Soc. 123 (2001) 9254–9259.
[44] M. Giel-Pietraszuk, A. Fedoruk-Wyszomirska, J. Barciszewski, Effect of high hydrostatic pressure on hydration and activity of ribozymes, Mol. Biol. Rep. 37 (2010) 3713–3719.
[45] H. Kaddour, J. Vergne, G. Hervé, M.-C. Maurel, High-pressure analysis of a hammerhead ribozyme from chrysanthemum chlorotic mottle viroid reveals two different populations of self-cleaving molecule, FEBS J. 278 (2011) 3739–3747.
[46] M. Giel-Pietraszuk, J. Barciszewski, Hydrostatic and osmotic pressure study of the RNA hydration, Mol. Biol. Rep. 39 (2012) 6309–6318.
[47] C. Schuabb, M. Berghaus, C. Rosin, R. Winter, Exploring the free energy and conformational landscape of tRNA at high temperature and pressure, ChemPhysChem 16 (2015) 138–146.
[48] J.C. Miner, A.A. Chen, A.E. García, Free-energy landscape of a hyperstable RNA tetraloop, Proc. Natl. Acad. Sci. U. S. A. 113 (2016) 6665–6670.
[49] C. Schuabb, N. Kumar, S. Pataraia, D. Marx, R. Winter, Pressure modulates the self-cleavage step of the hairpin ribozyme, Nat. Commun. 8 (2017) 14661.
[50] N. Kumar, D. Marx, Mechanistic role of nucleobases in self-cleavage catalysis of hairpin ribozyme at ambient versus high-pressure conditions, Phys. Chem. Chem. Phys. 20 (2018) 20886–20898.
[51] J.A. Doudna, T.R. Cech, The chemical repertoire of natural ribozymes, Nature 418 (2002) 222–228.
[52] G.F. Joyce, The antiquity of RNA-based evolution, Nature 418 (2002) 214–221.
[53] S. Nesbitt, L.A. Hegg, M.J. Fedor, An unusual pH-independent and metal-ion-independent mechanism for hairpin ribozyme catalysis, Chem. Biol. 4 (1997) 619–630.
[54] J.L. O'Rear, S. Wang, A.L. Feig, L. Beigelman, O.C. Uhlenbeck, D. Herschlag, Comparison of the hammerhead cleavage reactions stimulated by monovalent and divalent cations, RNA 7 (2001) 537–545.
[55] P.B. Rupert, A.R. Ferré-D'Amaré, Crystal structure of a hairpin ribozyme-inhibitor complex with implications for catalysis, Nature 410 (2001) 780–786.
[56] J.C. Cochrane, S.A. Strobel, Catalytic strategies of self-cleaving ribozymes, Acc. Chem. Res. 41 (2008) 1027–1035.
[57] J. Salter, J. Krucinska, S. Alam, V. Grum-Tokars, J.E. Wedekind, Water in the active site of an all-RNA hairpin ribozyme and effects of Gua8 base variants on the geometry of phosphoryl transfer, Biochemistry 45 (2006) 686–700.
[58] X. Zhuang, H. Kim, M.J.B. Pereira, H.P. Babcock, N.G. Walter, S. Chu, Correlating structural dynamics and function in single ribozyme molecules, Science 296 (2002) 1473–1476.
[59] D. Rueda, G. Bokinsky, M.M. Rhodes, M.J. Rust, X. Zhuang, N.G. Walter, Single-molecule enzymology of RNA: essential functional groups impact catalysis from a distance, Proc. Natl. Acad. Sci. U. S. A. 101 (2004) 10066–10071.
[60] T.J. Wilson, M. Nahas, L. Araki, S. Harusawa, T. Ha, D.M. Lilley, RNA folding and the origins of catalytic activity in the hairpin ribozyme, Blood Cells Mol. Dis. 38 (2007) 8–14.
[61] S. Liu, G. Bokinsky, N.G. Walter, X. Zhuang, Dissecting the multistep reaction pathway of an RNA enzyme by single-molecule kinetic fingerprinting, Proc. Natl. Acad. Sci. U. S. A. 104 (2007) 12634–12639.
[62] M.M. Rhodes, K. Reblova, J. Šponer, N.G. Walter, Trapped water molecules are essential to structural dynamics and function of a ribozyme, Proc. Natl. Acad. Sci. U. S. A. 103 (2006) 13380–13385.
[63] M. Martick, W.G. Scott, Tertiary contacts distant from the active site prime a ribozyme for catalysis, Cell 126 (2006) 309–320.
[64] N.G. Walter, Ribozyme catalysis revisited: is water involved? Mol. Cell 28 (2007) 923–929.
[65] P. Auffinger, Y. Hashem, Nucleic acid solvation: from outside to insight, Curr. Opin. Struct. Biol. 17 (2007) 325–333.
[66] J. Wang, P. Cieplak, P.A. Kollman, How well does a restrained electrostatic potential (RESP) model perform in calculating conformational energies of organic and biological molecules? J. Comput. Chem. 21 (2000) 1049–1074.
[67] A. Pérez, I. Marchán, D. Svozil, J. Šponer, T.E. Cheatham III, C.A. Laughton, M. Orozco, Refinement of the AMBER force field for nucleic acids: improving the description of alpha/gamma conformers, Biophys. J. 92 (2007) 3817–3829.
[68] M. Zgarbová, M. Otyepka, J. Šponer, A. Mládek, P. Banáš, T.E. Cheatham, P. Jurečka, Refinement of the Cornell et al. nucleic acids force field based on reference quantum chemical calculations of glycosidic torsion profiles, J. Chem. Theory Comput. 7 (2011) 2886–2902.
[69] C.S. Gaines, D.M. York, Ribozyme catalysis with a twist: active state of the twister ribozyme in solution predicted from molecular simulation, J. Am. Chem. Soc. 138 (2016) 3058–3065.
[70] M. Terrazas, I. Ivani, N. Villegas, C. Paris, C. Salvans, I. Brun-Heath, M. Orozco, Rational design of novel N-alkyl-N capped biostable RNA nanostructures for efficient long-term inhibition of gene expression, Nucleic Acids Res. 44 (2016) 4354–4367.
[71] J. Wang, Y. Xiao, Types and concentrations of metal ions affect local structure and dynamics of RNA, Phys. Rev. E 94 (2016) 1–6.
[72] C.S. Gaines, D.M. York, Model for the functional active state of the TS ribozyme from molecular simulation, Angew. Chem. Int. Ed. 56 (2017) 13392–13395.
[73] H. Chen, T.J. Giese, B.L. Golden, D.M. York, Divalent metal ion activation of a guanine general base in the hammerhead ribozyme: insights from molecular simulations, Biochemistry 56 (2017) 2985–2994.
[74] J. Šponer, G. Bussi, M. Krepl, P. Banáš, S. Bottaro, R.A. Cunha, A. Gil-Ley, G. Pinamonti, S. Poblete, P. Jurečka, N.G. Walter, M. Otyepka, RNA structural dynamics as captured by molecular simulations: a comprehensive overview, Chem. Rev. 118 (2018) 4177–4338.
[75] S. Bottaro, P. Banáš, J. Šponer, G. Bussi, Free energy landscape of GAGA and UUCG RNA tetraloops, J. Phys. Chem. Lett. 7 (2016) 4032–4038.
[76] P. Kührová, R.B. Best, S. Bottaro, G. Bussi, J. Šponer, M. Otyepka, P. Banáš, Computer folding of RNA tetraloops: identification of key force field deficiencies, J. Chem. Theory Comput. 12 (2016) 4534–4548.
[77] M. Zgarbová, P. Jurečka, P. Banáš, M. Havrila, J. Šponer, M. Otyepka, Noncanonical α/γ backbone conformations in RNA and the accuracy of their description by the AMBER force field, J. Phys. Chem. B 121 (2017) 2420–2433.
[78] P. Banáš, D. Hollas, M. Zgarbová, P. Jurečka, M. Orozco, T.E. Cheatham, J. Šponer, M. Otyepka, Performance of molecular mechanics force fields for RNA simulations: stability of UUCG and GNRA hairpins, J. Chem. Theory Comput. 6 (2010) 3836–3849.
[79] S. Haldar, P. Kührová, P. Banáš, V. Spiwok, J. Šponer, P. Hobza, M. Otyepka, Insights into stability and folding of GNRA and UNCG tetraloops revealed by microsecond molecular dynamics and well-tempered metadynamics, J. Chem. Theory Comput. 11 (2015) 3866–3877.
[80] V. Mlýnský, P. Kührová, M. Zgarbová, P. Jurečka, N.G. Walter, M. Otyepka, J. Šponer, P. Banáš, Reactive conformation of the active site in the hairpin ribozyme achieved by molecular dynamics simulations with ε/ζ force field reparametrizations, J. Phys. Chem. B 119 (2015) 4220–4229.
[81] C. Vega, J.L.F. Abascal, Simulating water with rigid non-polarizable models: a general perspective, Phys. Chem. Chem. Phys. 13 (2011) 19663–19688.
[82] C. Hölzl, P. Kibies, S. Imoto, R. Frach, S. Suladze, R. Winter, D. Marx, D. Horinek, S.M. Kast, Design principles for high-pressure force fields: aqueous TMAO solutions from ambient to kilobar pressures, J. Chem. Phys. 144 (2016) 144104.
[83] I.S. Joung, T.E. Cheatham, Determination of alkali and halide monovalent ion parameters for use in explicitly solvated biomolecular simulations, J. Phys. Chem. B 112 (2008) 9020–9041.
[84] B. Hess, C. Kutzner, D. van der Spoel, E. Lindahl, GROMACS 4: algorithms for highly efficient, load-balanced, and scalable molecular simulation, J. Chem. Theory Comput. 4 (2008) 435–447.
[85] M.J. Abraham, T. Murtola, R. Schulz, S. Páll, J.C. Smith, B. Hess, E. Lindahl, GROMACS: high performance molecular simulations through multi-level parallelism from laptops to supercomputers, SoftwareX 1-2 (2015) 19–25.
[86] S. Nosé, A unified formulation of the constant temperature molecular dynamics methods, J. Chem. Phys. 81 (1984) 511–519.
[87] W.G. Hoover, Canonical dynamics: equilibrium phase-space distributions, Phys. Rev. A 31 (1985) 1695–1697.

[88] M. Parrinello, A. Rahman, Polymorphic transitions in single crystals: a new molecular dynamics method, J. Appl. Phys. 52 (1981) 7182–7190.
[89] U. Essmann, L. Perera, M.L. Berkowitz, T. Darden, H. Lee, L.G. Pedersen, A smooth particle mesh Ewald method, J. Chem. Phys. 103 (1995) 8577–8593.
[90] B. Hess, H. Bekker, H.J.C. Berendsen, J.G.E.M. Fraaije, LINCS: a linear constraint solver for molecular simulations, J. Comput. Chem. 18 (1997) 1463–1472.
[91] Y. Sugita, Y. Okamoto, Replica-exchange molecular dynamics method for protein folding, Chem. Phys. Lett. 314 (1999) 141–151.
[92] D.J. Earl, M.W. Deem, Parallel tempering: theory, applications, and new perspectives, Phys. Chem. Chem. Phys. 7 (2005) 3910–3916.
[93] H. Lei, Y. Duan, Improved sampling methods for molecular simulation, Curr. Opin. Struct. Biol. 17 (2007) 187–191.
[94] D. Rastädter, M. Biswas, I. Burghardt, Molecular dynamics study of the controlled destabilization of an RNA hairpin structure by a covalently attached azobenzene switch, J. Phys. Chem. B 118 (2014) 8478–8488.
[95] J.B. Swadling, D.W. Wright, J.L. Suter, P.V. Coveney, Structure, dynamics, and function of the hammerhead ribozyme in bulk water and at a clay mineral surface from replica exchange molecular dynamics, Langmuir 31 (2015) 2493–2501.
[96] A. Patriksson, D. van der Spoel, A temperature predictor for parallel tempering simulations, Phys. Chem. Chem. Phys. 10 (2008) 2073–2077.
[97] T. Okabe, M. Kawata, Y. Okamoto, M. Mikami, Replica-exchange Monte Carlo method for the isobaric-isothermal ensemble, Chem. Phys. Lett. 335 (2001) 435–439.
[98] A. Luzar, D. Chandler, Hydrogen-bond kinetics in liquid, Nature 379 (1996) 55–57.
[99] D. van der Spoel, P.J. van Maaren, P. Larsson, N. Timneanu, Thermodynamics of hydrogen bonding in hydrophilic and hydrophobic media, J. Phys. Chem. B 110 (2006) 4393–4398.
[100] M.C. Stumpe, H. Grubmüller, Aqueous urea solutions: structure, energetics, and urea aggregation, J. Phys. Chem. B 111 (2007) 6220–6228.
[101] O. Markovitch, N. Agmon, Reversible geminate recombination of hydrogen-bonded water molecule pair, J. Chem. Phys. 129 (2008) 084505.
[102] A.M. Saitta, F. Datchi, Structure and phase diagram of high-density water: the role of interstitial molecules, Phys. Rev. E 67 (2003) 020201.
[103] S.J. Grabowski, T.M. Krygowski, Estimation of the proton position and the energy of O-H..O bridges in crystals from X-ray diffraction data, Tetrahedron 54 (1998) 5683–5694.
[104] S.J. Grabowski, Ab initio calculations on conventional and unconventional hydrogen bonds - study of the hydrogen bond strength, J. Phys. Chem. A 105 (2001) 10739–10746.
[105] K. Modig, B.G. Pfrommer, B. Halle, Temperature-dependent hydrogen-bond geometry in liquid water, Phys. Rev. Lett. 90 (2003) 075502.
[106] K. Wendler, J. Thar, S. Zahn, B. Kirchner, Estimating the hydrogen bond energy, J. Phys. Chem. A 114 (2010) 9529–9536.